Thermodynamically self-consistent theories of fluids interacting through short-range forces

C. Caccamo,* G. Pellicane, and D. Costa
Istituto Nazionale per la Fisica della Materia (INFM) and Dipartimento di Fisica, Università di Messina, Contrada Papardo, Salita Sperone 31, 98166 Messina, Italy

D. Pini
Istituto Nazionale per la Fisica della Materia (INFM) and Dipartimento di Fisica, Università di Milano, Via Celoria 16, 20133 Milano, Italy

G. Stell
Department of Chemistry, State University of New York at Stony Brook, Stony Brook, New York 11794-3400
(Received 5 May 1999; revised manuscript received 28 July 1999)

The self-consistent Ornstein-Zernike approximation (SCOZA), the generalized mean spherical approximation (GMSA), the modified hypernetted chain (MHNC) approximation, and the hierarchical reference theory (HRT) are applied to the determination of thermodynamic and structural properties, and the phase diagram of the hard-core Yukawa fluid (HCYF). We investigate different Yukawa-tail screening lengths λ, ranging from $\lambda=1.8$ (a value appropriate to approximate the shape of the Lennard-Jones potential) to $\lambda=9$ (suitable for a simple one-body modelization of complex fluids like colloidal suspensions and globular protein solutions). The comparison of the results obtained with computer simulation data shows that at relatively low λ's all the theories are fairly accurate in the prediction of thermodynamic and structural properties; as far as the phase diagram is concerned, the SCOZA and HRT are able to predict the binodal line and the critical parameters in a quantitative manner. At $\lambda=4$ some discrepancies begin to emerge in the performances of the different theoretical approaches: the MHNC remains, on the whole, reasonably accurate in predicting the energy and the contact value of the radial distribution function; the SCOZA predicts well the equation of state up to the highest λ values investigated. The GMSA and the MHNC underestimate and overestimate, respectively, the liquid coexisting density, while the SCOZA and HRT yield liquid branches that fall between the two former theoretical predictions, although both appear to overestimate the critical temperature somewhat. At higher λ's the GMSA and MHNC binodals further worsen, while the SCOZA appears to remain usefully predictive. In general, the predictions of all the theories tend to slightly worsen at low temperatures and high density. The determination of the freezing line, performed by means of a one-phase ''freezing criterion'' (due to other authors) is not particularly satisfactory within either the SCOZA or the MHNC; the GMSA prediction for the freezing line at $\lambda=7$ and 9 is instead able to follow in a qualitative manner the pattern of the solid-vapor coexistence line as determined through computer simulation studies. The necessity of further assessments of the freezing predictions is also discussed. Finally, versions of the GMSA, SCOZA, and HRT that can be expected to be more accurate for interactions with extremely short-ranged attractions are identified. [S1063-651X(99)10911-5]

PACS number(s): 61.20.Gy, 61.20.Ja

I. INTRODUCTION

The hard-core Yukawa fluid (HCYF) has been the object of a rather intense investigation in most recent years (see [1] for a review). One reason for such an interest is that for this model one has available analytic and semianalytic theories (see [1–6] and references quoted therein) that allow one a rapid investigation of its physical properties; on the other hand, the potential parameters can easily be adjusted so as to mimic more realistic interactions, such as, for instance, the Lennard-Jones potential [7]; the two circumstances allow then one to predict in a fairly easy, albeit approximate, manner the properties of a number of real fluids.

The simplicity of the model has also prompted the assessment of the performances of several theories against computer simulation data. Such comparisons have mainly concerned thermodynamic properties [8–10], with estimates of phase coexistence conditions and predictions of critical behavior [11–15]; in particular, the modified hypernetted chain (MHNC [16]) approximation and the semianalytic self-consistent Ornstein-Zernike approximation (SCOZA [4,5,15]) have been applied in the low-value regime of the Yukawa screening parameter λ [14,15], with a satisfactory reproduction of the liquid-vapor binodal line; the SCOZA also provides a good description of the critical point region, including the nonclassical critical exponent that describes liquid-vapor coexistence [15,17]. The liquid-vapor coexistence line and the critical exponents are also accurately described by the hierarchical reference theory (HRT [18–20]), which incorporates the renormalization-group treatment of the critical region.

These studies have, however, been restricted to some spe-

*Author to whom correspondence should be address. Electronic address: caccamo@vulcano.unime.it

cific cases, and no systematic investigation of the accuracy of different theories over wide ranges of temperatures, densities and Yukawa screening parameters λ has, to our knowledge, hitherto been performed. In particular, an assessment of the accuracy of various theoretical approaches at high λ is still lacking; such a parameter regime is worth investigating since it corresponds to very short-ranged potentials, a situation in which the phase diagram of the fluid undergoes profound modifications, with the disappearance of a stable liquid phase [11,12]. As documented in the current literature, a phase portrait of this kind is of particular interest for the description of complex fluids like colloidal suspensions and protein solutions (see Ref. [21], and references therein); it has been argued, in fact, that the location of the binodal line just below the sublimation line, a configuration in which the metastable critical point is very close to the vapor-solid phase transition boundary, might represent the most favorable condition for a controlled nucleation process in the fluid, and hence for a regular growth of crystals [21,22]. The latter circumstance is certainly of great interest in protein solutions; in these systems, in fact, the crystallization procedures do frequently fail to yield crystals of large enough size and quality to allow a confident diffraction study of the molecular structure [23].

In view of the above considerations, we have undertaken an extensive investigation of the thermodynamic and structural properties, as well as of the phase diagram, of the HCYF, by assessing at the same time the performances of the most advanced theories presently available (both semianalytic and iteratively solvable); we implement here a numerical solution procedure of a comprehensive form of the generalized mean spherical approximation (GMSA [2,24–26]), which also embodies, as additive equations, the thermodynamic consistency constraints descending from all the three routes connecting structure to thermodynamics in liquid-state theories [27]. The consistency is thus achieved only in terms of internal conditions. We also apply the MHNC theory, as well as simple versions of the SCOZA and the HRT; the solution schemes for these theories have been developed elsewhere by other authors.

Our analysis encompasses, in particular, λ values ranging from $\lambda \simeq 2$, roughly corresponding to the Lennard-Jones fluid, up to $\lambda \simeq 9$, a realistic screening length for HCYF modelizations of colloidal suspensions and protein solutions [12,28,29]. The determination of the binodal is performed according to conventional procedures. The freezing line is determined on the basis of a one-phase ''freezing criterion'' proposed by other authors [30]. Comparison is made, whenever possible, with phase diagrams obtained through computer simulation by other authors [11,12,15,31], supplemented by the production of a number of new simulation data for this same model.

The paper is organized as follows: theories and simulation schemes are described in Sec. II; the procedures for determining the lines of coexisting phases and the freezing line are briefly outlined in Sec. III. The results are reported and discussed in Sec. IV. Section V contains our conclusions.

II. MODEL, THEORIES, AND SIMULATION SCHEMES

We consider a fluid composed of hard-sphere particles of diameter σ, interacting through an attractive Yukawa tail; the interparticle potential is thus written as

$$v(r)=\infty, \quad r<\sigma,$$
$$v(r)=-\sigma\epsilon \exp[-\lambda(r-\sigma)]/r, \quad r\geqslant\sigma. \tag{1}$$

The properties of this model fluid are calculated in the context of the MHNC approximation and versions of the GMSA, the SCOZA, and the HRT, all of which are defined below.

As is well known, in the MHNC scheme [16], the Ornstein-Zernike equation

$$h(r)=c(r)+\rho\int c(|\mathbf{r}-\mathbf{r}'|)h(r')d\mathbf{r}', \tag{2}$$

where $g(r)$ is the radial distribution function (RDF) and $h(r)=g(r)-1$ and $c(r)$ are the pair and direct correlation function, respectively, is solved by means of the formally exact closure

$$g(r)=\exp[-\beta v(r)+h(r)-c(r)+B(r)]. \tag{3}$$

Here $B(r)$ is the bridge function of the system under study and $\beta=1/k_BT$.

We shall assume that the bridge function for the HCYF can be approximated by that of a hard-sphere fluid in the Percus-Yevick (PY) approximation. As usual in the MHNC scheme, we choose the hard-core diameter entering the definition of the PY bridge function so as to impose a (partial) thermodynamic consistency constraint on the theory.

Specifically, we require the equality of the isothermal compressibilities as calculated according to the virial and compressibility route [27]; that is,

$$\left(\beta\frac{\partial P^{\rm vir}}{\partial\rho}\right)_{T,\rho}=1-\rho\tilde{c}(q=0). \tag{4}$$

Here $\tilde{c}(q=0)$ is the $q=0$ limit of the Fourier transform of $c(r)$. The solution of the system of equations (2), (3) is obtained through the well-known Gillan algorithm [32].

In the GMSA [2,24–26] a closure to Eq. (2) is obtained by observing that, because of Eq. (1), one has

$$g(r)=0, \qquad r<\sigma, \tag{5}$$

and by assuming

$$c(r)=-\beta v(r)+K\exp[-z(r-\sigma)]/r, \qquad r\geqslant\sigma, \tag{6}$$

where $v(r)$ is given by Eq. (1), while K and z entering the Yukawa function in Eq. (6) are used as adjustable parameters in order to impose the internal thermodynamic consistency of the theory. Specifically, we impose in the GMSA the satisfaction of condition (4) and also

$$-\left(\frac{\partial F}{\partial V}\right)_T^U=P^{\rm vir}, \tag{7}$$

where the left-hand side of Eq. (7) is the pressure obtained from the energy route by differentiating the Helmholtz free energy F, whose excess part with respect to the hard-sphere

fluid F^{ex} is in turn obtained from the configurational energy U^{ex} through standard thermodynamic integration along an isochore path [27]; that is,

$$\beta F^{ex}(\rho)=\int_0^\beta U^{\mathrm{ex}}(\beta',\rho)d\beta'. \tag{8}$$

The isochore path integration starts from infinite temperature ($\beta=0$), corresponding to the hard-sphere limit of the HCYF. The hard-sphere fluid free energy is in turn obtained by integrating the equation of state along an isothermal path at infinite temperature starting from zero density up to the density of interest; the Yukawa parameters K and z are progressively adjusted along the path so as to reproduce the Carnahan-Starling [33] pressure and compressibility at each thermodynamic point. The hard-sphere Helmholtz free energy has thus the Carnahan-Starling value.

We have implemented the solution of the GMSA in a fully numerical manner. Specifically, we have used Eq. (6) as a closure relation in an iterative solution procedure of the integral equation (2); the rationale for such a choice, which does not make use of any of the more direct semianalytic solution schemes available in the literature, is that conditions (4) and (7) require in any case a numerical search of the consistency parameters; we have thus found it advantageous to incorporate their fulfilment in the same numerical procedure that solves Eqs. (2) and (6).

It is worthwhile at this point to note that Stell, Høye, and their coauthors have used the term GMSA in a generic sense, applied to a family of approximations, all of which have the common feature of supplementing the $-\beta v(r)$ term appearing in a direct correlation function $c(r)$ outside the core with Yukawa terms. In some versions of the GMSA (for example, those that have already been used to describe fluids of charged spheres and dipolar spheres [24,34]), the amplitudes and ranges of the Yukawa terms are adjusted to yield self-consistency with thermodynamics given by prescribed equations of state that have been predetermined, rather than by equations of state that are determined through the imposition of self-consistency, as is the case here. This latter form of the GMSA (which can also be regarded as a SCOZA, as noted below) is more demanding computationally, especially in the version used here that requires self-consistency among the energy, virial, and compressibility routes to thermodynamics. The work reported here is the first quantitative study of this particular version for the HCYF. An alternative version, introduced in Ref. [4], that also involves consistency among the same three routes, has not yet been assessed.

The term SCOZA is also used by Høye and Stell in a generic sense to apply to approximations in which one or more state-dependent parameters are introduced into the relation between $c(r)$ and $-\beta v(r)$ in such a way that thermodynamic self-consistency gives rise to a differential equation for one of the parameters, the solution of which yields the thermodynamics of the system. In the version of SCOZA used here, there is only one parameter A, multiplying the $-\beta v(r)$ term outside the core; but there is a second term, also of Yukawa form, that represents the contribution to $c(r)$ outside the core from the hard-sphere core itself,

$$c(r)=-A\beta v(r)+K_{\mathrm{HS}}\exp[-z_{\mathrm{HS}}(r-\sigma)]/r, \qquad r\geqslant\sigma, \tag{9}$$

where we use the subscript HS to signify that K_{HS} and z_{HS} depend only on the presence of the hard-sphere core, independent of $v(r)$. The K_{HS} and z_{HS} are predetermined by setting $v(r)=0$ in Eq. (9) and requiring that both the compressibility and the virial route to thermodynamics yield the Carnahan-Starling equation of state for a hard-sphere fluid. The A in Eq. (9) is then obtained by requiring that the compressibility and energy routes yield the same thermodynamics, which requires the consistency condition

$$-\frac{\partial}{\partial\beta}\tilde{c}(q=0)=\frac{\partial^2}{\partial\rho^2}\left(\frac{U^{\mathrm{ex}}}{V}\right)_T. \tag{10}$$

This in turn induces a consistency condition upon $A(\rho,\beta)$ in the form of a partial-differential equation that must be solved numerically. For the Yukawa fluid considered here, this is made simpler by the fact that within the closure (9) the relation between the inverse reduced compressibility $1-\rho\tilde{c}(q=0)$ and the excess internal energy U^{ex} can be determined analytically [2,3]. The solution procedure has been described in detail in Ref. [15].

The designations SCOZA and GMSA as used by Høye and Stell are not mutually exclusive. In fact the GMSA investigated here is identical to the more comprehensive version of the SCOZA developed by Høye and Stell in Ref. [5] that ensures self-consistency with respect to the virial equation as well as the energy and compressibility equations.

For the sake of a more complete overview of theoretical results, we also include the results of some calculations performed within the HRT; this approach, which does not have the structure of the other liquid-state integral-equation theories, embodies the correct renormalization-group behavior as the liquid-vapor critical point is approached.

In the HRT the interparticle potential is first split into a short-range, repulsive contribution $v_R(r)$ and a longer-ranged, attractive one $w(r)$. For the hard-core plus tail interaction considered here this is done trivially. The attractive part is then turned on in a gradual fashion by introducing a modified interaction $w_Q(r)$, such that its Fourier components with wave vectors smaller than a certain cutoff Q are vanishing. In the resulting Q *system*, long-range fluctuations with characteristic length $L>1/Q$ are then strongly inhibited. As Q evolves from $Q=\infty$, the interaction takes on its components of longer and longer wavelengths, until in the limit $Q\to 0$ the fully interacting system is recovered. The corresponding evolution of the Helmholtz free energy is described by the exact equation

$$\frac{\partial}{\partial Q}\left(\frac{\beta\mathcal{F}_Q}{V}\right)=\frac{Q^2}{4\pi^2}\ln\left(1+\frac{\beta\tilde{w}(Q)}{\tilde{\mathcal{C}}_Q(Q)}\right), \tag{11}$$

where $\tilde{w}(k)$ is the Fourier transform of the attractive interaction, and $\mathcal{F}_Q$ and $\tilde{\mathcal{C}}_Q(k)$ are straightforwardly related to the Helmholtz free energy F_Q and to the Fourier transform of the direct correlation function $c_Q(r)$ of the Q system. Equation (11) is closed by resorting to an approximation similar to Eq. (9). Specifically, we assume

$$g_Q(r)=0, \qquad r<\sigma, \tag{12}$$

$$\mathcal{C}_Q(r)=B_Q\beta w(r)+c_R(r), \quad r\geqslant\sigma,$$

where c_R is the direct correlation function of the hard-sphere fluid, as given, for instance, by the Verlet-Weis parametrization [35]; and B_Q is determined so as to satisfy the compressibility sum rule

$$\tilde{\mathcal{C}}_Q(k=0)=\frac{\partial^2}{\partial\rho^2}\left(-\frac{\beta\mathcal{F}_Q}{V}\right). \tag{13}$$

This can be regarded as a consistency condition between the compressibility route and a route (different from all the above-mentioned ones) in which the thermodynamics is determined from the Helmholtz free energy as obtained from Eq. (11). The latter yields then a partial-differential equation for $\mathcal{F}_Q$, which is integrated numerically starting from $Q=\infty$ down to $Q\rightarrow 0$. We refer the reader to the related literature for more details [18–20].

Finally, a number of conventional constant-temperature, constant-volume Monte Carlo (MC [36]) simulations have been performed. As detailed in Sec. IV, quite large system samples, enclosed in cubic boxes with periodic boundary conditions, are employed in this context, in order to get accurate estimates of various thermodynamic quantities of interest. Whenever necessary long-range corrections have been adopted in order to correct for truncation effects at the box boundaries on the radial distribution function. The isothermal compressibility is also calculated by generating the equation of state of the fluid through a series of constant volume simulations along an isotherm, with an accurate sampling centered at the density of interest.

III. THEORETICAL PROCEDURES FOR THE DETERMINATION OF THE PHASE DIAGRAM

The liquid-vapor coexistence curve is determined straightforwardly in the HRT, since the conditions of chemical equilibrium between the two coexisting phases are implemented by the theory itself. In fact, below the critical temperature this approach yields a vanishing inverse compressibility and rigorously flat isotherms inside a certain domain of the phase plane, which is then identified with the coexistence region.

In the GMSA, MHNC, and SCOZA the determination of the liquid-vapor coexistence line is instead performed by equating the chemical potential at equal temperature and pressures on the liquid and vapor side of the binodal, respectively. The chemical potential is obtained from the Helmholtz free energy calculated either by integrating the pressure along an isothermal path, or by integrating the configurational energy with respect to the inverse temperature along an isochore path [see Eq. (8)].

In implementing such a procedure, it happens that both the MHNC and the GMSA solution algorithms fail to converge at a thermodynamic consistent solution in the critical point region; as a consequence, we cannot display results for the binodal from these two theories on a restricted temperature range close to the critical temperature. In light of earlier results that have already come out of both theoretical and computational studies of HNC-type theories, this difficulty in locating a binodal and critical point may well be intrinsic to such theories rather than an artifact of our numerical procedure (in the HNC approximation, for example, there appears to be no critical point at which the compressibility computed via the compressibility relation diverges [37,38]). On the other hand, the study of the analytic structure of the GMSA made in [5] strongly suggests that the GMSA is an approximation for which the binodal is well defined in the critical region and at a critical point, which can in principle be located with arbitrarily high precision, just as in the SCOZA.

By adopting an approach originally proposed in Ref. [30], we also locate the onset of freezing in our HCYF by monitoring the behavior of the multiparticle residual entropy, defined as

$$\Delta s\equiv s_{\rm ex}-s_2, \tag{14}$$

where $s_{\rm ex}$ is the the excess entropy per particle of the system in units of the Boltzmann constant, and

$$s_2=-\frac{1}{2}\rho\int\{g(r)\ln[g(r)]-g(r)+1\}d\mathbf{r}. \tag{15}$$

According to previous results reported in the literature [30,39], it turns out that the vanishing of Δs acts as a quite sensitive indicator of the freezing transition in several one-component fluids. The possibility that this same condition can be associated with structural rearrangements that herald other types of phase separations has also been discussed elsewhere [40].

IV. RESULTS AND DISCUSSION

In what follows we shall measure the distance, the density, and the temperature, in σ, σ^{-3}, and ϵ/k_B units, respectively. Other quantities of interest are similarly expressed in the appropriate reduced units.

A. Thermodynamic and structural properties

The GMSA, MHNC, SCOZA [15], and HRT predictions for the HCYF with $\lambda=1.8$ are compared with one another and with MC results obtained with the use of 2000 particles. Comparison with previous computer simulation data [8,10], obtained with a few hundred particles is also reported. Three different temperatures, $T=1.0$, 1.5, and 2.0, have been investigated along the same isochore $\rho=0.80$; as will appear in Sec. IV B, the first state point ($T=1.0,\rho=0.8$) falls deep inside the liquid pocket of the system; at $T=1.50$ the system is instead already in a supercritical dense phase. Thermodynamic results are shown in Fig. 1.

Several comparisons between all four theories and simulation have been performed also for the case $\lambda=4$, along the isochore $\rho=0.816$, a density that falls just before the freezing line [11] (see below) and at temperatures ranging from inside the liquid pocket of the phase diagram ($0.5<T<0.625$) up to a supercritical state ($T=1.0$). MC simulations are performed on a sample composed of 1500 atoms. Results are displayed in Fig. 2.

More extensive investigations have been performed for $\lambda=9$. GMSA, SCOZA, and MHNC predictions are assessed against MC data (obtained on a sample of 512 particles)

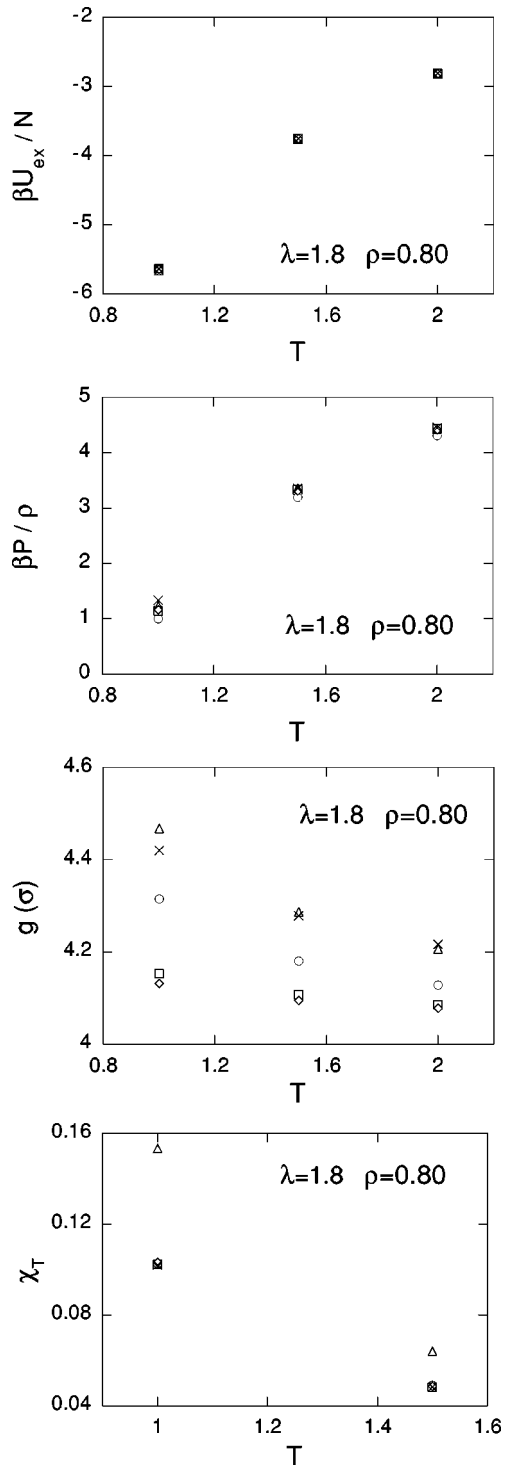

FIG. 1. Internal energy per particle, equation of state $g(\sigma)$, and the compressibility (in reduced units) for the HCYF with $\lambda = 1.8$. Symbols: circles, MHNC; triangles, GMSA; squares, SCOZA; diamonds, HRT; crosses, MC simulations. Error bars on the simulation data are smaller than the relative marker size.

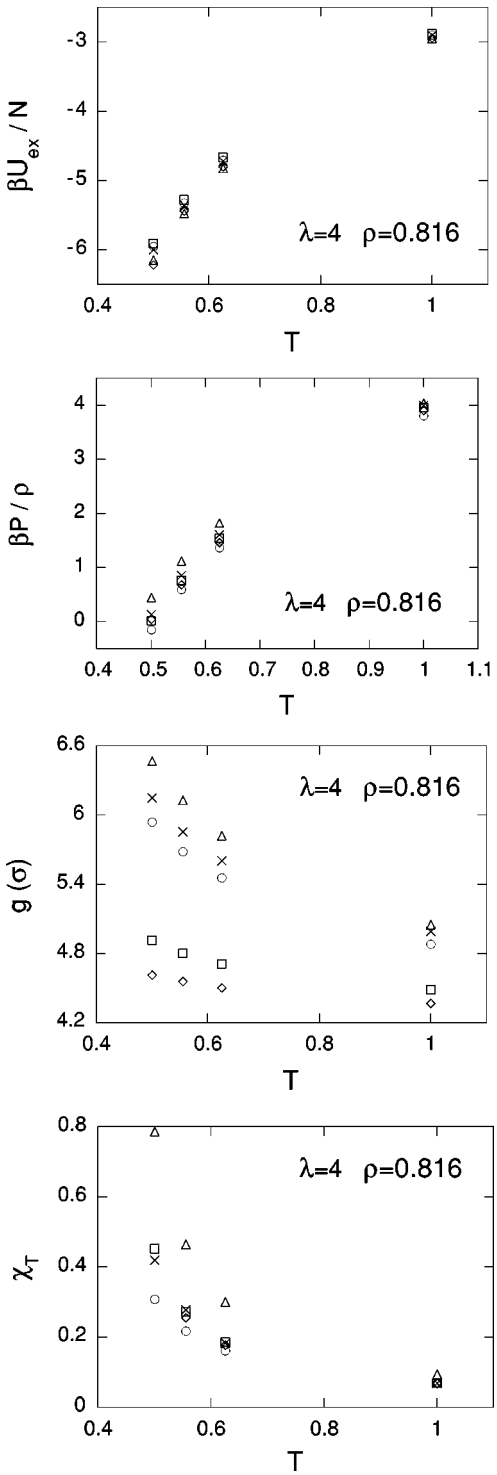

FIG. 2. Same as Fig. 1 for the case $\lambda = 4$.

along the isochores $\rho = 0.5$ and $\rho = 0.7$, from $T = 0.80$, well above the sublimation line (as estimated by other authors [12]) to $T = 0.45$. Results are visualized in Fig. 3. Radial distribution functions are collectively shown for all λ's investigated in Fig. 4.

One first important feature of the results previously reported is the accuracy of the MHNC approach (which in our scheme is implemented with the use of PY bridge functions) in the prediction of both thermodynamic and structural quantities of the HCYF on a very wide range of Yukawa screening parameters. In particular, the MHNC turns out to be able to reproduce in a practically quantitative manner the simulation data for the energy at all the λ's investigated, and on a very wide range of temperatures and densities. The same theory is slightly less accurate in predicting the pressure, the compressibility, and the contact values of the radial distribution function. It seems remarkable that such a good perfor-

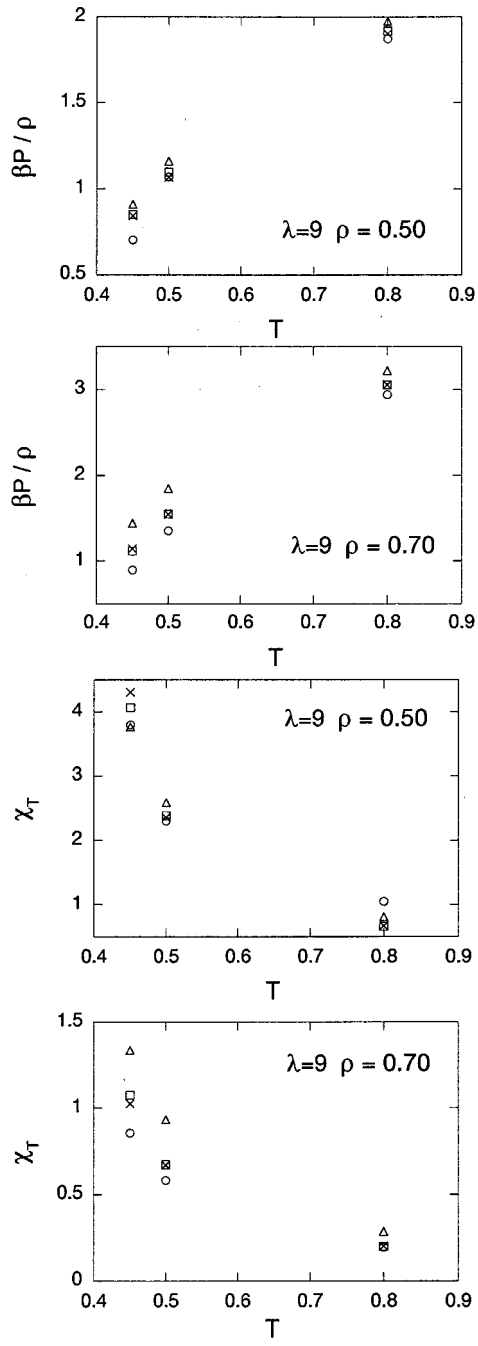

FIG. 3. Equation of state and compressibility factor for the HCYF with $\lambda=9$. Results along the isochores $\rho=0.50$ (top panels) and $\rho=0.70$ (bottom panels) are displayed. Symbols as in Fig. 1.

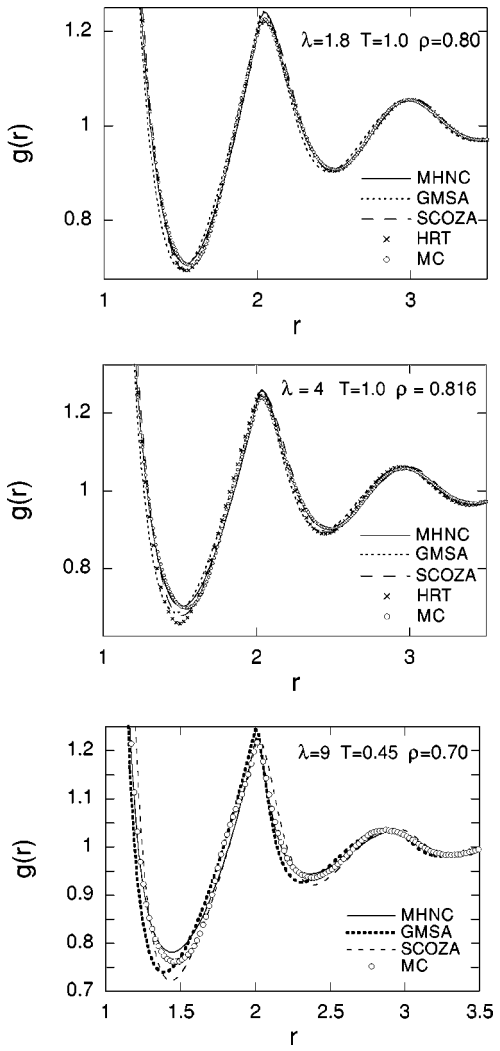

FIG. 4. Radial distribution function for the HCYF with various λ's; thermodynamic state points and symbols, see figures.

mance can be obtained by imposing a single thermodynamic consistency constraint.

The SCOZA, on the other hand, is the best of the theories for directly predicting the equation of state, and it turns out to retain its accuracy in this regard at the larger λ's, even at high density and low temperature. The SCOZA $g(r)$ is reasonably good at low λ's but shows a trend toward overestimating the amplitude of the oscillations, and also toward moderately losing the phase when λ increases; the main deficiency is the poor estimate of the contact RDF at high λ. In relation to this point, it is to be noted that, although this theory embodies an accurate representation of the hard-sphere fluid properties at the level of the Carnahan-Starling equation of state, thermodynamic consistency is imposed only between fluctuation and energy pressures, without any explicit control on the virial (a quantity directly related to the contact RDF). This perhaps accounts for the poor $g(\sigma)$ estimates at high λ's.

The GMSA embodies in principle a full thermodynamic consistent treatment; it does not seem, however, that this is sufficient to make the theory accurate at all λ's. The fact that the compressibility predictions are relatively less accurate than the pressure and the contact RDF, together with the increasingly poor representation of $g(r)$ at large r, indicate that, despite the link to two consistency constraints, the adopted closure is not able to entirely cope with the interplay between short- and long-range effects in the interaction potential. This is perhaps not surprising in light of the fact that the two parameters K and z of the GMSA shown in Eq. (6) are being asked to play an even more comprehensive thermodynamic role than the three SCOZA parameters A, K_{HS}, and z_{HS}, in Eq. (9). In the SCOZA, the K_{HS} and z_{HS} are dedicated to accurately and self-consistently taking into account the hard-core contribution to the thermodynamics, so that A need only accommodate itself to the energy-compressibility self-consistency of the thermodynamics that

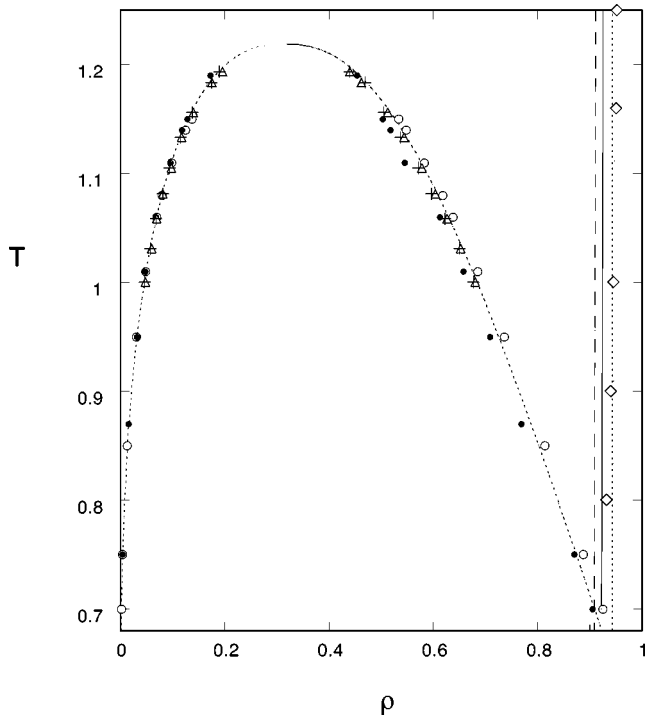

FIG. 5. Theoretical and finite-size scaling MC results for the phase diagram of the HCYF with $\lambda = 1.8$. Liquid-gas coexistence: dotted line, SCOZA; triangles, HRT; full circles, GMSA; open circles, MHNC; pluses, finite-size scaling MC of Ref. [15]. $\Delta s = 0$ locus (freezing): dotted line, SCOZA; full line, MHNC; dashed line, GMSA; diamonds: freezing line for $\lambda = 2$ according to density-functional calculations of Ref. [43].

results from the additional presence of the soft tail of the pair potential. In the GMSA, on the other hand, the K and z must assure that the thermodynamics of both the hard-core contribution to $v(r)$ and its soft Yukawa tail together yield full virial-energy-compressibility self-consistency. This appears to be too demanding a task to be met with high accuracy by the simple form of the single Yukawa term in Eq. (6).

The HRT is accurate in the prediction of thermodynamic quantities up to $\lambda = 4$. We have verified, however, that beyond this value its accuracy decreases, as we shall see below, where other HRT results will be reported. Since Eq. (11) is exact, this must be regarded as a consequence of the approximation intrinsic in the closure relation (12). The latter appears then to become less and less reliable as λ increases.

B. Phase diagram

The phase diagram at $\lambda = 1.8$ is shown in Fig. 5. It appears that all the theories reproduce rather satisfactorily the binodal curve as obtained in Ref. [15] through a finite-size scaling Monte Carlo simulation technique [41].

In particular, as already reported in Ref. [14], the binodal is well predicted by the MHNC, although the density of the coexisting liquid phase is slightly overestimated. The opposite behavior is shown by the GMSA. The results from the SCOZA, previously obtained elsewhere [15], and from the HRT, turn out to be ''bracketed'' by the two former theories, and appear as the most satisfactory. Both the SCOZA below the critical point [15,17] and the HRT yield nonclassical critical exponents; their estimates for the exponent β that describes the shape of the binodal curve are 7/20 ($=0.35$) and 0.345, respectively. The best renormalization-group estimate of this value is in the neighborhood of 0.327 [42]. The performances of the different theories on the vapor branch of the binodal are also very accurate, as seen in Fig. 5.

The critical parameters predicted by the various theories at $\lambda = 1.8$ are reported in Table I. As noted in Sec. II, the MHNC and GMSA iterative algorithms become unable to yield a thermodynamic consistent solution for temperatures too close to the critical one. For this reason the GMSA and the MHNC entries are deduced from a power-law interpolation of the available points performed with the nonclassical critical exponent $\beta = 0.32$, together with the application of the law of rectilinear diameters. At $\lambda = 1.8$ the SCOZA [15] and the HRT are in quantitative agreement with simulation. The GMSA is also quite accurate. The MHNC (also investigated in Ref. [14]) is quite good but slightly inferior to the other three theories.

Some of the theoretical trends emerging at $\lambda = 1.8$ herald more pronounced deviations from the simulation results at $\lambda = 4$. This is visible in Fig. 6, where it appears that, on the liquid side of the binodal, the MHNC moderately overestimates and the GMSA sensibly underestimates, respectively, the densities of the coexisting phases. The SCOZA is again in between the two theories; the same is true also for the HRT, but only up to intermediate temperatures. In fact, above $T = 0.55$ the HRT binodal is external to the MHNC one. The critical temperature and density predicted by the

TABLE I. Theoretical and simulation critical point parameters.

	$\lambda = 1.8$		$\lambda = 4.0$		$\lambda = 7.0$	
	T_{cr}	ρ_{cr}	T_{cr}	ρ_{cr}	T_{cr}	ρ_{cr}
MC	1.212 (2)[a]	0.312 (2)[a]	0.576 (6)[b]	0.377 (21)[b]	0.411 (2)[c]	0.50 (2)[c]
GMSA	1.199	0.312	0.576	0.324		
MHNC	1.193	0.326	0.581	0.412		
MHNC[d]	1.21	0.28				
HRT	1.214	0.312	0.599	0.394	0.435	0.424
SCOZA	1.219	0.314	0.591	0.3895	0.419	0.4575

[a]Finite-size scaling MC simulation of Ref. [15].
[b]Gibbs-ensemble MC simulations of Ref. [11].
[c]Gibbs-ensemble MC simulations of Ref. [12].
[d]MHNC calculations with Verlet-Weis bridge functions of Ref. [14].

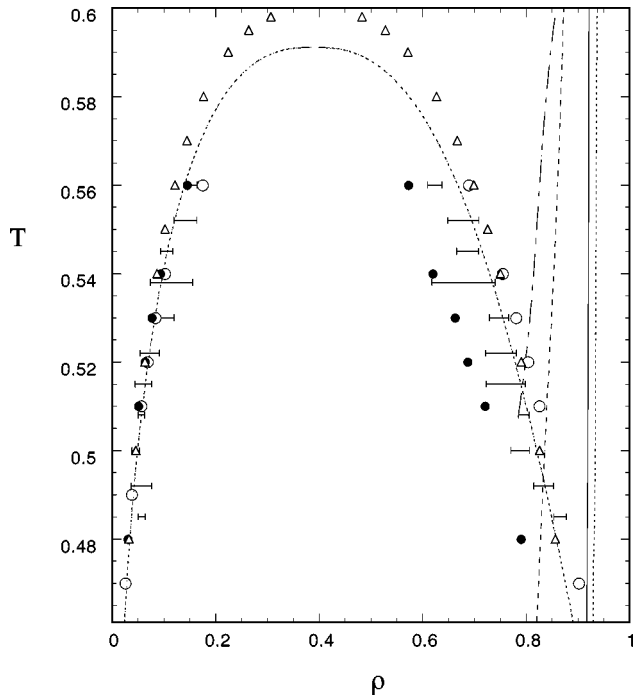

FIG. 6. Theoretical and simulation results for the phase diagram of the HCYF with $\lambda=4$. Liquid-gas coexistence: horizontal bars, Gibbs-ensemble MC results of Ref. [11]; other symbols as in Fig. 5. $\Delta s=0$ locus (freezing line): dash-dotted line, results of Ref. [12] for $\lambda=3.9$; other symbols as in Fig. 5.

different theories are still quite satisfactory (see Table I).

The case with $\lambda=7$ is now considered. The related results are shown in Fig. 7. Note that the computer simulation results, known from previous studies [12], show the shift of the binodal line beneath the sublimation line, a circumstance that implies the metastability of the liquid-vapor equilibrium.

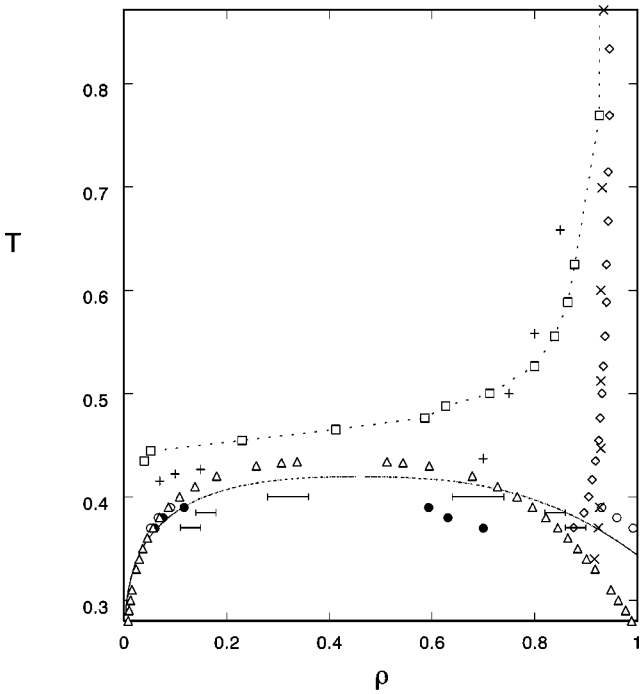

FIG. 7. Phase diagram for the HCYF with $\lambda=7$. Liquid-gas coexistence: horizontal bars, Gibbs-ensemble MC results of Ref. [12]; other symbols as in Fig. 5. $\Delta s=0$ locus: diamonds, SCOZA; pluses, GMSA; crosses, MHNC; dashed line with squares, sublimation line of Ref. [12].

Some of the theories now show considerable discrepancies with respect to the Gibbs ensemble Monte Carlo (GEMC) data of Ref. [12]. The GMSA result, in particular, appears poor on both the liquid and the vapor branch of the coexistence line. The MHNC now sensibly overestimates on one side, and underestimates on the other, the coexistence liquid and vapor density, respectively. As a result, the simulation binodal falls well inside the MHNC one.

The SCOZA, as for the other λ's, is between the MHNC and the GMSA, and maintains a reasonable agreement with the GEMC results. The HRT too is between the MHNC and the GMSA at low temperature, but its critical temperature is higher than the SCOZA one. Note that the GEMC results are themselves subject to some uncertainty; in fact, the location of the binodal in the critical region via simulation is a demanding task, and simulation results using finite-size scaling techniques that help assure quantitative precision, were only available to us from [15] for the $\lambda=1.8$ case.

We now focus our attention on the freezing line. As noted in Sec. III, previous studies by other authors [30,39,40] indicate that the locus of vanishing multiparticle residual entropy, $\Delta s=0$, corresponds with remarkable accuracy to the freezing line of several model fluids. A detailed discussion of the physical meaning of the $\Delta s=0$ condition in relation to its ''coincidence'' with the freezing and other coexistence lines, can be found in Refs. [30,40]. Here we restrict ourselves to examining the related results for the HCYF by performing whenever possible a comparison with the simulation results.

Calculations of the $\Delta s=0$ *loci* performed according to different the theories are reported in Figs. 5–7. As we can first see in Fig. 5, at $\lambda=1.8$ the MHNC, GMSA, and SCOZA results fall quite close to each other, and to density-functional theory [43]. A calculation of the freezing line performed by using the Hansen-Verlet freezing criterion [44] with the SCOZA structure factor as input (whose results are not displayed in the figure), yields a freezing line that descends almost vertically down to a density $\rho=0.94$. The triple-point temperature, determined from the intersection of the freezing line with the binodal line, is considerably below the critical one, thus indicating the existence of a very well-defined liquid pocket.

It is interesting to note that on the vapor side of the binodal the MHNC and GMSA $\Delta s=0$ locus practically falls on the estimated coexisting vapor density line. We could not verify whether anything similar happens for densities close to the liquid branch of the binodal, because of numerical difficulties in that density region. A trend of Δs to vanish seems, however, conjecturable on the basis of the results shown in Fig. 8 (see Ref. [40] for a discussion about the possible meaning of multiple vanishing of the multiparticle residual entropy).

Results for the $\Delta s=0$ loci at $\lambda=4$ are shown in Fig. 6. We can see that the GMSA falls fairly close to the computer simulation line of freezing, by moderately overestimating the freezing density. The MHNC and the SCOZA lines are instead still almost vertical, as in the $\lambda=1.8$ case. We have verified that calculations with the Hansen-Verlet criterion do yield a freezing line hardly different from the one at λ

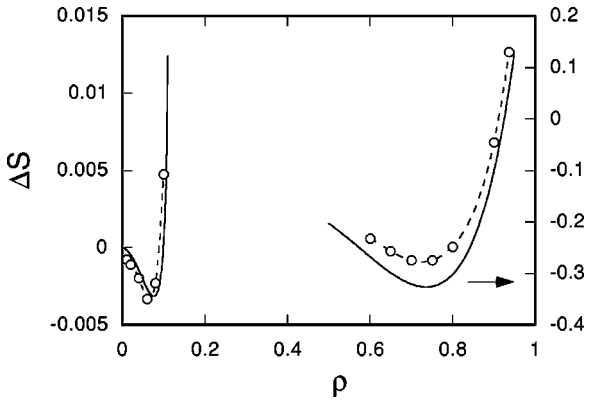

FIG. 8. Residual entropy Δs for the HCYF with $\lambda=1.8$ and $T=1.08$ as a function of the density. Symbols: dashed line with circles, GMSA; full line, MHNC. Note the scale on the right indicated by the arrow.

$=1.8$. Similar remarks to those for the $\lambda=1.8$ case can be made for the vanishing of Δs along the vapor side of the binodal, as obtained within the MHNC and the GMSA.

The MHNC and SCOZA $\Delta s=0$ loci at $\lambda=7$ (see Fig. 7) hardly differ from those at lower λ's. The GMSA curve, instead, falls now very close to the simulation freezing line, although it is not able to follow the trend to flatten of the sublimation curve at low temperatures. It is interesting to note, however, that a portion of the GMSA $\Delta s=0$ locus can be obtained also in the vapor region, and this is located well above the coexisting vapor density. We could not follow the $\Delta s=0$ behavior at intermediate densities due to numerical instability problems. An almost flat interpolation between the two branches could, however, be reasonably assumed. It is also interesting to note that at $\lambda=7$ the GMSA binodal is located at temperatures that are sensibly smaller than those of the $\Delta s=0$ locus, in a way that resembles the relative location of the binodal vs the sublimation lines obtained through simulation.

Finally, as shown in Fig. 9, the GMSA locus at $\lambda=9$ shows a moderate dependence on the temperature at intermediate densities, and qualitatively resembles the sublimation line predicted by simulation. The MHNC $\Delta s=0$ locus in

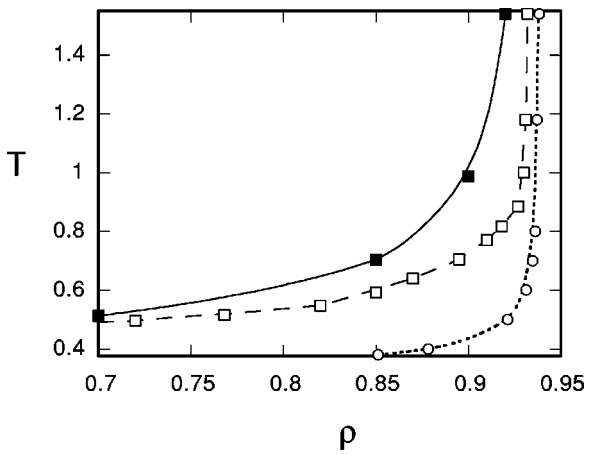

FIG. 9. $\Delta s=0$ locus for the HCYF with $\lambda=9$. Symbols: full squares: GMSA; open squares, sublimation line of Ref. [12]; open circles: MHNC. The lines are guides for the eye.

comparison stops at considerably higher densities and is located at lower temperatures. It is also interesting to note that at $\lambda=7$ the GMSA binodal is located at temperatures that are sensibly lower than those of the $\Delta s=0$ locus, in a way that resembles the relative location of the binodal vs the sublimation lines obtained through simulation.

V. CONCLUSIONS

Thermodynamic and structural properties, as well as the phase diagram of the HCYF have been investigated for different values of the Yukawa screening parameter λ. Calculations performed in the MHNC, in the GMSA with consistency constraints from all the three routes (fluctuations, virial, and energy) from structure to thermodynamics, in the SCOZA, and in the HRT, have been compared with one another and with new and accurate computer simulation data obtained for high λ's.

The results presented here document the accuracy of the MHNC scheme in the prediction of both thermodynamic and structural quantities of the HCYF in a very wide range of Yukawa screening parameters. The SCOZA, on the other hand, is the best of the theories for directly predicting the equation of state, and it turns out to retain its accuracy in this regard at the larger λ's, even at high density and low temperature, which the other theories do not. The GMSA is reasonably accurate for the thermodynamic quantities and for $g(\sigma)$ only at low λ's. The HRT appears to be on a comparable level of accuracy.

As far as the phase diagram is concerned, at low λ's ($\lambda=1.8$), that is, when the potential is not very short-ranged, all the theories investigated reproduce with considerable accuracy the simulation phase diagram. At higher λ's ($\lambda\geqslant 4$), significant differences emerge in the performances of the various theories. The SCOZA is able to maintain good agreement with the computer simulation binodal, while the GMSA and the MHNC somewhat underestimate and overestimate, respectively, the coexistence density on the liquid branch; the HRT also yields too high a critical temperature starting from $\lambda=4$.

In view of the good performances of the MHNC, especially in predicting the structural properties of the HCYF, it seems worth trying to use accurate bridge functions, as those, for instance, obtainable from the bridge-functional approach based on the fundamental measure theory recently proposed by Rosenfeld (see Ref. [46] for a recent review). Calculations in this direction are in progress.

The success of SCOZA in predicting the equation of state, despite its relative lack of contact-value accuracy, is also quite striking. This turns out to be especially true in the liquid-vapor critical region and leads to the most accurate overall binodals among the theories we have considered. The fact that the GMSA has not represented an overall improvement as a result of its more accurate $g(\sigma)$ via imposition of virial-theorem self-consistency suggests that one should consider other means of incorporating that theorem. One way of doing this is to let the range as well as the amplitude of the term relating $c(r)$ and $v(r)$ differ from that of $v(r)$, as discussed in Sect. IV of [4]. Another way to do this is suggested by the observation [45] that the function

$$c(r)+\beta v(r)=h(r)-\ln g(r)+B(r) \tag{16}$$

for a Lennard-Jones type fluid has the exact large-r form $Kh^2(r)$, which suggests using

$$c(r)=-\beta v(r)+K_1 h^2(r)+B_{\mathrm{HS}}(r), \tag{17}$$

with K_1 and the diameter of the hard-sphere bridge function $B_{\mathrm{HS}}(r)$ adjusted to yield compressibility-energy-virial self-consistency. This scheme could equally well be regarded as an alternative version of the GMSA.

Although the HRT does not impose self-consistency among any of the three routes considered here, in its current implementation it resorts to a closure relation for the direct correlation function similar to that used in SCOZA [see Eqs. (9) and (12)], the main difference being the way in which the amplitude of the interaction contribution to $c(r)$ is determined. In particular, in both theories the profile of the ''excess'' direct correlation function $c(r)-c_{\mathrm{HS}}(r)$ outside the core is forced to follow $v(r)$ at large as well as at small r's. Using an expression more suited to represent the structure of $c(r)$ even when it is expected to be very different from that of $v(r)$, as is the case with a very short-ranged potential, appears to be a possible way of obtaining improved results also in the context of the HRT.

We turn now to the ''freezing criterion.'' The freezing line, as determined either from the vanishing of the residual multiparticle entropy Δs, or according to the Hansen-Verlet criterion, is not as satisfactorily predicted as the binodal line. In fact, the SCOZA and the MHNC yield a freezing density that is not significantly sensitive to the variation of the potential range, as is known, instead, to be the case from simulation studies. These latter show that at $\lambda \geqslant 7$ the sublimation line runs above the (metastable) binodal line, with the liquid-vapor critical point falling just beneath the vapor-solid transition line.

However, the GMSA $\Delta s=0$ turns out to be able to follow in a qualitative manner the modification of the freezing line with λ. In particular, at $\lambda=9$, the locus of vanishing residual multiparticle entropy shifts well above the liquid-vapor coexistence line in a manner that fairly mimics the relative location of the freezing and binodal line in this λ regime.

It should be noted that all of the integral-equation approximations we have studied here have only been fully defined for the fluid state and not the solid state. As a result, strictly speaking, these approximations are silent as to the location of the triple point and freezing line. They are also silent with regard to the location of the vapor-solid coexistence curve defined for temperatures below the triple-point temperature. Although we believe it is of considerable interest to combine the results of the fluid-state approximations with freezing criteria, such as the $\Delta s=0$ criterion, to predict freezing and sublimation lines that can be compared to simulation results, the quality of such predictions clearly cannot be used to rank the relative accuracy of the fluid theories *per se*.

A natural way of extending the integral-equation theories we consider to the solid phase is to incorporate in the theories the form that one expects of the direct correlation function for the crystal symmetry (or symmetries, if more than one is in contention) associated with the expected solid. One can then find the most stable phase for each ρ and T by comparing the free energy of the solid, or solids in contention, with the fluid free energy, and selecting the minimum. This procedure is at the heart of those versions of density-functional theory that incorporate Ornstein-Zernike formalism. For the versions of the GMSA and the SCOZA considered here this would entail using in place of the Yukawa form of Eqs. (6) and (9) an appropriately parametrized functional form that is consistent with the symmetry of the solid into which the HCYF is expected to freeze. For the MHNC or the modified SCOZA/GMSA given respectively by Eqs. (3) and (17), one would instead use a $B_{\mathrm{HS}}(r)$ appropriate to solid symmetry to characterize the solid phase.

Such generalizations represent a formidable computational challenge, but our results here indicate that, on the basis of currently available freezing criteria, fluid-state integral-equation theories are not able to yield comparable results for fluid-solid phase separation when the attractive term becomes extremely short-ranged.

ACKNOWLEDGMENTS

D.P. acknowledges the support of the National Science Foundation for his work while at Stony Brook. G.S. acknowledges support by the Division of Chemical Sciences, Office of Science, Office of Energy Research, U.S. Department of Energy. D.C. acknowledges the support of the project on protein crystallization PROCRY of the Istituto Nazionale Fisica della Materia. C.C., D.C., and G.P. wish to thank the Istituto Tecniche Spettroscopiche of CNR in Messina for making available local computing facilities.

[1] C. Caccamo, Phys. Rep. **274**, 1 (1996).
[2] E. Waisman, Mol. Phys. **25**, 45 (1973).
[3] J.S. Høye and G. Stell, Mol. Phys. **32**, 195 (1976); **32**, 209 (1976).
[4] J.S. Høye and G. Stell, J. Chem. Phys. **67**, 439 (1977).
[5] J.S. Høye and G. Stell, Mol. Phys. **52**, 1071 (1984).
[6] D. Duh and L. Mier-Y-Terán, Mol. Phys. **90**, 373 (1997).
[7] E.N. Rudisill and P.T. Cummings, Mol. Phys. **68**, 629 (1990); Y.V. Kalyuzhnyi and P.T. Cummings, *ibid.* **87**, 1459 (1996).
[8] D. Henderson, E. Waisman, J.L. Lebowitz, and L. Blum, Mol. Phys. **35**, 241 (1978).
[9] J. Konior and C. Jedrzejek, Mol. Phys. **55**, 187 (1985); J. Konior, *ibid.* **68**, 129 (1989).
[10] C. Rey, L.J. Gallego, and L.E. Gonzàlez, J. Chem. Phys. **96**, 6984 (1992).
[11] E. Lomba and N.E. Almarza, J. Chem. Phys. **100**, 8367 (1994).
[12] M.H.J. Hagen and D. Frenkel, J. Chem. Phys. **101**, 4093 (1994).
[13] L. Mederos and G. Navascués, J. Chem. Phys. **101**, 9841 (1994).
[14] C. Caccamo, G. Giunta, and G. Malescio, Mol. Phys. **84**, 125 (1995).
[15] D. Pini, G. Stell, and N.B. Wilding, Mol. Phys. **95**, 483 (1998).
[16] Y. Rosenfeld and N.W. Ashcroft, Phys. Rev. A **20**, 1208

(1979).
[17] D. Pini, G. Stell, and R. Dickman, Phys. Rev. E **57**, 2862 (1998); J.S. Høye, D. Pini, and G. Stell (unpublished).
[18] A. Parola and L. Reatto, Phys. Rev. Lett. **53**, 2417 (1984); Phys. Rev. A **31**, 3309 (1985); A. Meroni, A. Parola, and L. Reatto, *ibid.* **42**, 6104 (1990); M. Tau, A. Parola, D. Pini, and L. Reatto, Phys. Rev. E **52**, 2644 (1995).
[19] A. Parola and L. Reatto, Adv. Phys. **44**, 211 (1995).
[20] L. Reatto, in *New Approaches to Old and New Problems in Liquid State Theory*, edited by C. Caccamo, J.P. Hansen, and G. Stell, Vol. 529 of *NATO Advanced Studies Insitute Series B: Physics* (Kluwer, Dordrecht, 1999).
[21] P.R. ten Wolde and D. Frenkel, Science **277**, 1975 (1997).
[22] M. Muschol and F. Rosenberger, J. Chem. Phys. **107**, 1953 (1997).
[23] A. McPherson, *Preparation and Analysis of Protein Crystals* (Krieger, Malabar, FL, 1982).
[24] J.S. Høye, J.L. Lebowitz, and G. Stell, J. Chem. Phys. **61**, 3253 (1974).
[25] J.S. Høye and L. Blum, J. Stat. Phys. **19**, 317 (1978).
[26] L. Blum, J. Stat. Phys. **22**, 661 (1980).
[27] J.P. Hansen and I.R. McDonald, *Theory of Simple Liquids*, 2nd ed. (Academic Press, London, 1986).
[28] D. Rosenbaum, P.C. Zamora, and C.F. Zukoski, Phys. Rev. Lett. **76**, 150 (1995).
[29] M. Malfois, F. Bonneté, L. Belloni, and A. Tardieu, J. Chem. Phys. **105**, 3290 (1996).
[30] P.V. Giaquinta and G. Giunta, Physica A **187**, 145 (1992); P.V. Giaquinta, G. Giunta, and S. Prestipino Giarritta, Phys. Rev. A **45**, R6966 (1992).
[31] E.J. Meijer and F. Elazhar, J. Chem. Phys. **106**, 4678 (1997).
[32] M.J. Gillan, Mol. Phys. **38**, 1781 (1979).
[33] N.F. Carnahan and K.E. Starling, J. Chem. Phys. **51**, 635 (1969).
[34] G. Stell and S.F. Sun, J. Chem. Phys. **63**, 5333 (1975); J.S. Høye and G. Stell, *ibid.* **67**, 524 (1977).
[35] L. Verlet and J.J. Weis, Phys. Rev. A **5**, 939 (1972); D. Henderson and E.W. Grundke, J. Chem. Phys. **63**, 601 (1975).
[36] M.P. Allen and D.J. Tildesley, *Computer Simulation of Liquids* (Clarendon, Oxford, 1993).
[37] J.S. Høye, E. Lomba, and G. Stell, Mol. Phys. **79**, 523 (1993). Note especially the discussion in Secs. 4 and 5 and the references cited therein.
[38] L. Belloni, J. Chem. Phys. **98**, 8080 (1993).
[39] F. Saija, P.V. Giaquinta, G. Giunta, and S. Prestipino Giarritta, J. Phys.: Condens. Matter **6**, 9853 (1994); C. Caccamo, Phys. Rev. B **51**, 3387 (1995).
[40] P.V. Giaquinta, G. Giunta, and G. Malescio, Physica A **250**, 91 (1998).
[41] N.B. Wilding and A.D. Bruce, J. Phys.: Condens. Matter **4**, 3087 (1992).
[42] J. Zinn-Justin, *Quantum Field Theory and Critical Phenomena* (Clarendon, Oxford, 1983).
[43] M. Renkin and J. Hafner, J. Chem. Phys. **94**, 541 (1991).
[44] J.P. Hansen and L. Verlet, Phys. Rev. **184**, 151 (1969).
[45] G. Stell, in *Modern Theoretical Chemistry, Vol. 5A: Statistical Mechanics*, edited by B. Berne (Plenum, New York, 1977), see Eqs. (14)–(16).
[46] Y. Rosenfeld, in *New Approaches to Old and New Problems in Liquid State Theory* (Ref. [20]).